From small scale variability to mesoscale stability in surface ocean pH: implications for air-sea CO₂ equilibration

Louise Delaigue[1], Gert-Jan Reichart[1,2], Chris Galley[3,4], Yasmina Ourradi[1] and Matthew P. Humphreys[1]

[1]Department of Ocean Systems (OCS), NIOZ Royal Netherlands Institute for Sea Research, PO Box 59, 1790 AB Den Burg (Texel), the Netherlands
[2]Department of Earth Sciences, Utrecht University, Utrecht, the Netherlands.
[3]Department of Earth Sciences, Memorial University of Newfoundland, St. John's, NL, A1B 3X5, Canada
[4]Department of Earth and Environmental Sciences, University of Ottawa, Ottawa, ON, K1N 6N5, Canada

Correspondence to: Louise Delaigue (louise.delaigue@nioz.nl)

Abstract. One important aspect of understanding ocean acidification is the nature and drivers of pH variability in surface waters on smaller spatial (i.e., areas up to 100 km²) and temporal (i.e., days) scales. However, there has been a lack of high-quality pH data at sufficiently high resolution. Here, we describe a simple optical system for continuous high-resolution surface seawater pH measurements. The system includes a PyroScience pH optode placed in a flow-through cell directly connected to the underway supply of a ship through which near-surface seawater is constantly pumped. Seawater pH is measured at a rate of 2 to 4 measurements min^{-1} and is cross-calibrated using discrete carbonate system observations (total alkalinity, dissolved inorganic carbon and nutrients). This setup was used during two research cruises in different oceanographic conditions: the North Atlantic Ocean (December-January 2020) and the South Pacific Ocean (February-April 2022). Our findings reveal fine-scale fluctuations in surface seawater pH across the North Atlantic and South Pacific Oceans. While temperature is a significant abiotic factor driving these variations, it does not account for all observed changes. Instead, our results highlight the interplay between temperature, biological activity, and water masses on pH. Notably, the variability differed between the two regions, suggesting differences in the dominant factors influencing pH. In the South Pacific, biological processes appeared to be mostly responsible for pH variability, while in the North Atlantic, additional abiotic and biotic factors complicated the correlation between expected and observed pH changes. Although surface seawater pH exhibited fine-scale variations, it remained relatively stable over a 24-hour cycle due to reequilibration with atmospheric CO₂. Thus, for the regions and time periods studied, ocean basin-scale analyses based on discrete samples collected during traditional research cruise transects would still capture the necessary variability for global CO₂ cycle assessments and their implications.

1 Introduction

Ocean chemistry is changing due to the uptake of anthropogenic CO₂ from the atmosphere (DeVries, 2022). The uptake of atmospheric CO₂ by the ocean's surface causes a rise in the ocean's hydrogen ion concentration, a process commonly referred to as ocean acidification. As a result, the hydrogen ion concentration of surface ocean seawater has increased by 30-40%, which corresponds to a pH decrease of approximately 0.1 since around 1850 (Gattuso et al., 2015; Jiang et al., 2019; Orr et al., 2005). These changes have already significantly impacted marine organisms, especially marine calcifiers (Doney et al., 2020; Gattuso et al., 2015; Osborne et al., 2020), and pH is projected to decline by ~0.3 by 2100 (Figuerola et al., 2021).

To understand these impacts and the underlying mechanisms more precisely, high-resolution studies have significantly advanced our understanding of the upper ocean's carbon cycle. However, gaps remain, particularly at fine spatio-temporal scales (e.g., variability over hours and a few kilometers). At these scales, changes in pH over short time periods can be an important control on the ocean's buffering capacity and response to CO₂ uptake, highlighting the need for

45   further detailed observations (Cornwall et al., 2013; Egilsdottir et al., 2013; James et al., 2020;
46   Qu et al., 2017; Wei et al., 2022).
47

48   Advancements in the last decade and a half have enhanced the capacity for accurate and precise
49   in-situ pH measurements. For example, Martz et al. (2010) developed an autonomous sensor
50   tailored for continuous deployment in marine environments that allows recording of high-
51   resolution pH fluctuations. Autonomous surface vehicles in coastal upwelling systems have also
52   been used to capture intricate partial pressure of CO_2 ($p$$CO_2$) and pH dynamics, even in complex
53   environments where rapid biogeochemical changes occur due to natural phenomena like
54   upwelling (Chavez et al., 2018; Cryer et al., 2020; Possenti et al., 2021). Staudinger et al. (2018)
55   also developed an optode system capable of simultaneously measuring oxygen, carbon dioxide,
56   and pH in seawater. This system was designed for extended deployment (i.e. days) in marine
57   environments, enabling continuous monitoring (with measurement intervals between 1 second
58   and 1 hour) of these parameters. Additionally, Sutton et al. (2019) detailed the implementation of
59   autonomous seawater $p$$CO_2$ and pH time series from 40 surface buoys, broadening the scope of
60   observations at fixed time series sites. Staudinger et al. (2019) introduced fast and stable optical
61   pH sensor materials specifically for oceanographic applications, enhancing the ability to measure
62   pH under various environmental conditions.
63

64   These technological advancements have facilitated significant scientific progress. Field
65   measurements conducted using submersible spectrophotometric sensors have revealed fine-scale
66   variations in pH in coastal waters and shed light on localized acidification processes (Cornwall et
67   al., 2013). The implementation of autonomous seawater $p$$CO_2$ and pH time series as described by
68   Sutton et al. (2019) has enhanced our ability to characterize sub-seasonal variability in the ocean.
69   These efforts represent important progress that can be built upon to further understand fine-scale
70   ocean dynamics.
71

72   Fine spatio-temporal scale variability in surface ocean pH is hard to capture because it is driven
73   by a complex interplay of processes, including physical mixing, biological activity (i.e.
74   photosynthesis and respiration), thermal variability, and air-sea CO_2 fluxes (Faassen et al., 2023;
75   Hofmann et al., 2011; Price et al., 2012). Physical mixing moderates surface oceanic pH by
76   redistributing dissolved CO_2, nutrients, and heat throughout the water column. Mixing also
77   mitigates extreme pH fluctuations by diluting surface concentrations of CO_2 during periods of
78   high biological activity or temperature-induced CO_2 release (Egea et al., 2018; Li et al., 2019).
79   Photosynthetic activity can decrease CO_2, leading to an increase in pH during daylight hours,
80   while respiration dominates at night, releasing CO_2 and lowering pH (Fujii et al., 2021; Jokiel et
81   al., 2014). Warmer waters decrease CO_2 solubility and increase pH, while cooler waters increase
82   solubility, promoting CO_2 uptake and decreasing pH, although the timescale of these processes
83   differs, with some changes occurring instantaneously and others after equilibration (Zeebe &
84   Wolf-Gladrow, 2001). Instantaneous changes are driven by physical and chemical reactions,
85   while equilibration processes involve longer-term adjustments such as air-sea gas exchange and
86   the mixing of surface waters with deeper layers (Emerson & Hedges, 2008). Increased
87   atmospheric CO_2 boosts oceanic CO_2 uptake, lowering pH, while reduced atmospheric CO_2
88   would decrease oceanic CO_2, raising pH (Caldeira & Wickett, 2005; Orr et al., 2005). Although
89   each of these processes has its distinct impact on pH, their combined effects regulate the ocean's
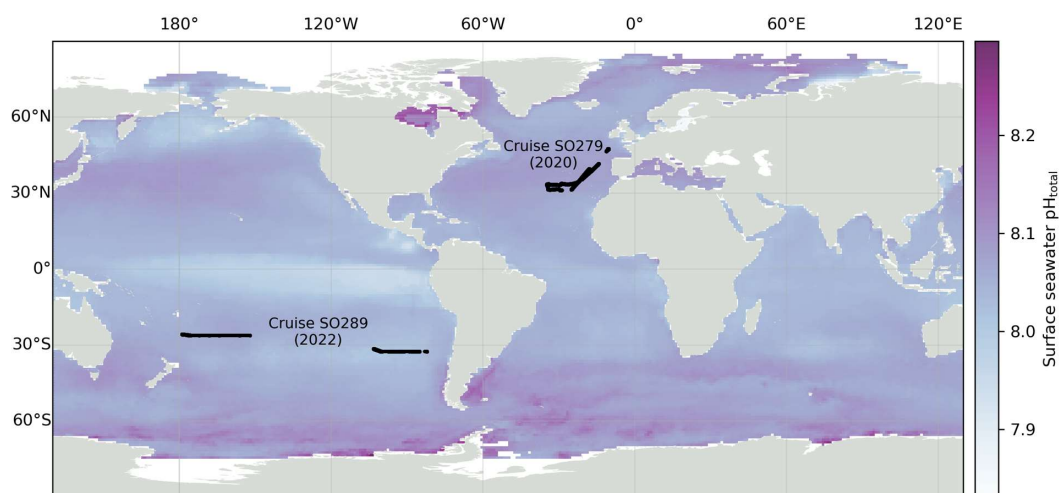90   carbon cycle and its interaction with the atmosphere.

91
92   Recent studies on air-sea CO_2 equilibration timescales have highlighted significant regional
93   variations, particularly between the North Atlantic and South Pacific Oceans (Jones et al., 2014).
94   In the North Atlantic, deeper mixed layers and unstable oceanic conditions lead to longer
95   equilibration timescales compared to temperate or tropical regions, ranging from 3 to 6 months
96   for the average North Atlantic latitude, and up to 18 months for regions above 55 °N (Jones et
97   al., 2014). Cooler temperatures at higher latitudes increase CO_2 solubility, resulting in higher
98   dissolved inorganic carbon (DIC), and upwelling brings DIC and total alkalinity (TA)-rich deep
99   waters to the surface (Wu et al., 2019). These factors further increase the amount of CO_2 that
100 needs to equilibrate with the atmosphere, further prolonging equilibration times. The South
101 Pacific, with its shallower mixed layers and higher average temperatures, facilitates shorter
102 equilibration times and enhances CO_2 uptake rates (i.e. 3 to 4 months; Jones et al., 2014). Wu et
103 al. (2019) also showed that high biological productivity in these areas significantly impacts DIC,
104 potentially reducing surface DIC more quickly.

105
106 Here, we investigate how surface seawater pH varies on fine spatio-temporal scales (i.e areas up
107 to 100 km^2, and days) across different ocean basins (i.e., North Atlantic and South Pacific
108 Oceans) and identify abiotic and biotic factors driving these variations. We use direct, high-
109 frequency measurements of surface seawater pH and estimate TA to resolve the rest of the
110 carbonate system. These data are used to analyse how key biogeochemical processes, such as
111 temperature, hydrodynamic mixing and biological activity, influence fine-scale spatio-temporal
112 variability in pH.

113 **2 Materials and Procedures**

114 **2.1 Study areas**

115
116 **Figure 1. Locations of pH measurements during two oceanographic cruises used in this study: SO279 in the**
117 **North Atlantic (December 2020) and SO289 in the South Pacific (February-April 2022). Surface seawater**
118 **pH$_{total}$ for December 2022 from the OceanSODA product is shown in the background (Gregor & Gruber,**
119 **2020).**
120

121 Two datasets from separate oceanic regions were used: research expeditions SO279 in the North
122 Atlantic Ocean and SO289 in the South Pacific Ocean, both on the German R/V Sonne (Fig. 1).
123
124 Expedition SO279 in December 2020, conducted in the Azores Region of the North Atlantic
125 Ocean (Fig. 1), was part of the NAPTRAM research program investigating the transport
126 pathways of plastic and microplastic debris (Beck et al., 2021). The data collection included
127 discrete samples from the CTD rosette (n=77; Delaigue et al., 2021a), with measurements of
128 DIC, TA and nutrients (silicate, phosphate ammonium, nitrite, and nitrate + nitrite); discrete
129 samples from the underway water system (UWS; n=51; Delaigue et al., 2021b) also measuring
130 these parameters; and a high-resolution UWS timeseries of ocean surface pH (over 43,000
131 datapoints; Delaigue et al., 2021c).
132
133 The South Pacific GEOTRACES Cruise SO289, from Valparaiso (Chile) to Noumea (New
134 Caledonia) under the GEOTRACES GP21 initiative, was conducted between 18 February and 08
135 April, 2022 (Fig. 1; Achterberg et al., 2022). The data collection also included discrete carbonate
136 chemistry and nutrient samples from the CTD rosette (n=395; Delaigue, Ourradi, Ossebar, et al.,
137 2023), discrete samples from the UWS (n=32; Delaigue, Ourradi, et al., 2023a) and another high-
138 resolution UWS timeseries of ocean surface pH from the optode system (over 78,000 datapoints;
139 Delaigue, Ourradi, et al., 2023b).

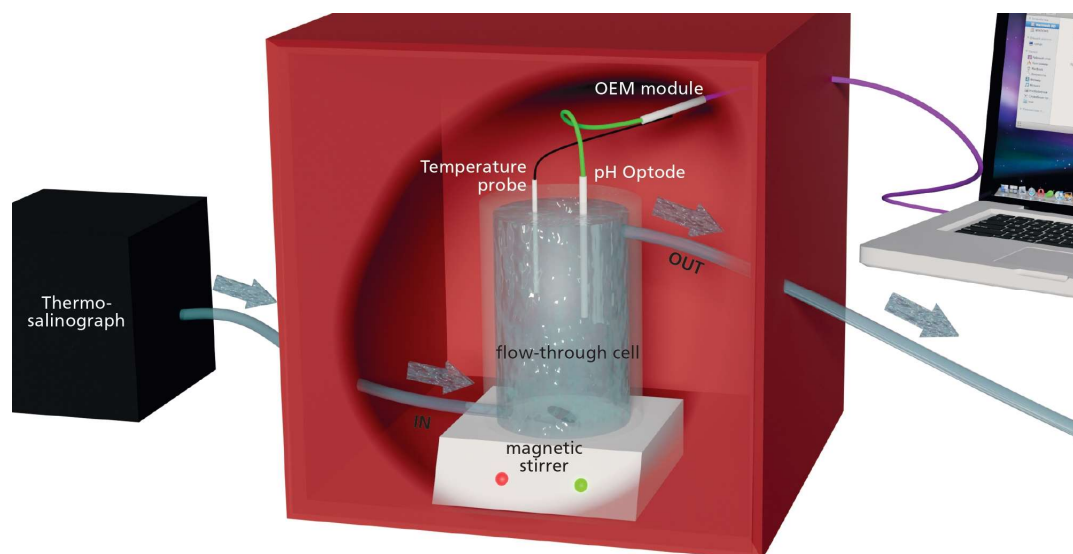**2.2 Integrated Shipboard Optode System for Continuous pH Measurements**

141 We used a pH optode (PHROBSC-PK8T, for pH range 7.0 – 9.0 on the total scale; PyroScience
142 GmbH), made of a robust cap adapter fiber with a stainless-steel tip (length=10cm,
143 diameter=4mm) and disposable plastic screw cap with an integrated pH sensor. The optode was
144 connected to a meter combined with a pressure-stable optical connector (optical feed-through;
145 OEM module Pico-pH-SUB; PyroScience GmbH; Fig. 2). Briefly, the optical pH sensor is
146 constructed using the PyroScience REDFLASH technology, which uses a pH neutral reference
147 indicator and a pH responsive luminescent dye. These elements are activated using a specifically
148 tuned orange-red light with a wavelength ranging between 610-630 nm, which triggers a bright
149 luminescence emission in the near-infrared (NIR) band, spanning from 760-790 nm. At elevated
150 pH, the fluorescence from the pH marker is diminished, leaving only the NIR emission of the
151 reference indicator noticeable. As the acidity increases, the pH marker is protonated, which
152 results in a heightened NIR luminescence that is detected along with the emissions of both
153 indicators. The measurement approach uses red excitation light modulated in a sinusoidal
154 manner, leading to a similar modulation of the NIR emission, albeit with a phase discrepancy.
155 This phase variation is registered by the PyroScience OEM module and subsequently converted
156 into a total pH measurement.
157
158 Automatic temperature compensation of the optical pH sensor was achieved using a flexible
159 Teflon-coated temperature probe (Pt100 Temperature Probe, PyroScience GmbH; Fig. 2)
160 soldered onto the OEM module. The optode was placed in a closed flow-through cell directly
161 connected to the underway supply of the ship through which seawater was pumped at a constant
162 rate (6 L/min for SO279 and 9 L/min for SO289) and stirred using a magnetic stirrer (Fig. 2).
163 The entire setup was kept inside a closed box to isolate the optical instrument from any other
164 light source (Fig. 2). All seawater first went through a thermo-salinograph close to the water

source, which also measured salinity, temperature and chlorophyll-a fluorescence (chl-a), before
going through the pH setup (Fig. 2).

Figure 2. Schematic representation of the optical continuous pH measurement system. Arrows indicate the direction of flow-through tubing. The system consists of the following components: a thermo-salinograph; a flow-through cell; a magnetic stirrer; a fiber-based pH optode; a flexible Teflon-coated temperature probe; a fiber-optic meter OEM module Pico-pH-SUB and a portable computer. All elements inside the red box are in the dark to avoid any light disturbance.

2.3 Initial calibration and underway measurements

Direct measurements of surface water (~3 m depth) pH were carried out at a frequency of 2 measurements min^{-1} for the North Atlantic cruise and 4 measurements min^{-1} for the South Pacific cruise.

A one-point calibration of the temperature probe was performed against a thermometer inside a water bath (Lauda Ecoline RE106). A two-point calibration of the pH sensor was performed using PyroScience pH buffer capsules (pH 2 or pH 4 for the acidic calibration point, pH 10 or pH 11 for the basic calibration points). Buffers were prepared by dissolving each capsule's powder into 100 mL MilliQ water. A pH offset adjustment was made using certified reference material (CRM, batches #189, #195 and #198; provided by Andrew Dickson, Scripps Institution of Oceanography).

2.4 Discrete sampling and analysis for other CO₂ parameters

The underway seawater system was sub-sampled from the cell every 12 hours via silicone tubing for TA and DIC following an internationally established protocol (Dickson et al., 2007). TA was sampled in Azlon™ HDPE wide neck round 150 mL bottles filled to the neck and poisoned with 50 μL saturated $HgCl_2$. DIC was sampled into Labco Exetainer® 12 ml borosilicate vials and

192   poisoned with 15 µL saturated $HgCl_2$. Samples were stored at 4 °C whenever possible and kept
193   in the dark until analysis.
194
195   All TA and DIC analysis was carried out at the Royal Netherlands Institute for Sea Research,
196   Texel (NIOZ). The analysis was calibrated using certified reference material (CRM, batches
197   #189, #195 and #198; provided by Andrew Dickson, Scripps Institution of Oceanography). TA
198   was determined using a Versatile INstrument for the Determination of Total inorganic carbon
199   and titration Alkalinity (VINDTA 3C #017 and #014, Marianda, Germany). The instrument
200   performed an open-cell, potentiometric titration of a seawater subsample with 0.1 M
201   hydrochloric acid (HCl). Results were then recalculated using a modified least-squares fitting as
202   implemented by Calkulate v3.1.0 (Humphreys and Matthews, 2024). DIC concentrations were
203   determined using either the VINDTA system (SO279 samples and part of SO289 samples) or the
204   QuAAtro Gas Segmented Continuous Flow Analyzer (CFA, SEAL Analytical; SO289 samples).
205   Briefly, the VINDTA measures DIC by acidifying a seawater sample, which releases CO_2 that is
206   then quantified through a coulometric titration cell. Similarly, the QuAAtro CFA uses
207   acidification to liberate CO_2, which then discolours a slightly alkaline phenolphthalein pink
208   coloured solution which is measured spectrophotometrically at 520 nm (Stoll et al., 2001).
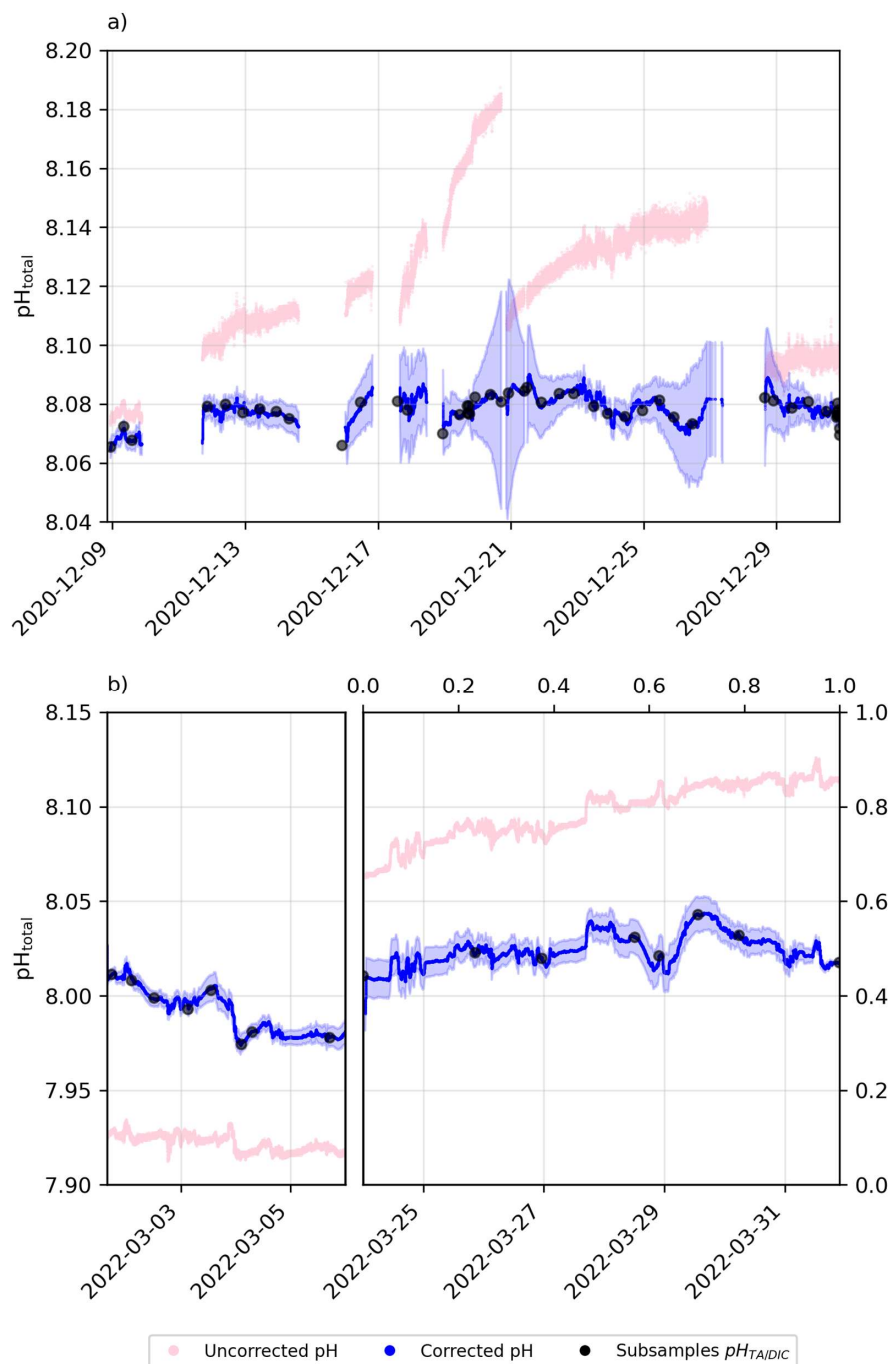209
210   For cruise SO279, nutrient samples were gathered using 60 mL syringes made of high-density
211   polyethylene, which were connected to a three-way valve by tubing, drawing directly from the
212   CTD-rosette bottles to avoid air exposure. Immediately upon collection, the samples were taken
213   to the laboratory for processing, where they were filtered through a dual-layer filter with pore
214   sizes of 0.8 and 0.2 µm. All samples were stored at -20°C in a freezer except Si, which were
215   stored at 4°C in a cold room until analysis back at NIOZ. Nutrients were analysed using a
216   QuAAtro Continuous Flow Analyser. Measurements were made simultaneously on four channels
217   together Si, PO_4, NH_4, NO_3, and NO_2. All measurements were calibrated with standards diluted
218   in low nutrient seawater (LNSW) in the salinity range of the stations (approx. 34 – 37) to ensure
219   that analysis remained within the same ionic strength. Prior to analysis, all samples were brought
220   to laboratory temperature in about one to two hours. To avoid gas exchange and evaporation
221   during the runs with NH_4 analysis, all vials including the calibration standards were covered with
222   Parafilm under tension before being placed into the auto-sampler, so that the sharpened sample
223   needle easily penetrated through the film leaving only a small hole. Silicate samples were
224   measured separately on a TRAACS Gas Segmented Continuous Flow Analyser (manufactured
225   by Bran+Lubbe, now SEAL Analytical) following Strickland and Parsons (1972). A sampler rate
226   of 60 samples per hour was also used for all analyses. Calibration standards were diluted from
227   stock solutions of the different nutrients in 0.2 µm filtered LNSW diluted with de-ionised water
228   to obtain approximately the same salinity as the samples and were freshly prepared every day.
229   This diluted LNSW was also used as the baseline water for the analysis and in between the
230   samples. Each run of the system had a correlation coefficient of at least 0.9999 for 10 calibration
231   points. The samples were measured from the lowest to the highest concentration, i.e., from
232   surface to deep waters in order to reduce carry-over effects. Concentrations were recorded in µM
233   at an average container temperature of 23.0 °C and later converted to µmol/kg by dividing the
234   recorded concentration by the sample density, calculated following Millero and Poisson (1981).
235
236   For cruise SO289, nutrient analysis was carried out on seawater from every Niskin bottle
237   triggered at various depths during each cast. The seawater was transferred into 15 mL

238   polypropylene vials. Each container and its cap were rinsed three times with seawater before
239   filling. If immediate analysis was not possible, samples were stored in a fridge at 4 °C in the
240   dark. Macro nutrients were analyzed onboard using a segmented flow injection analysis with a
241   Seal Analytical QUAATRO39 auto-analyzer that includes an XY2-autosampler. For nanomolar
242   nutrient analysis, a modified setup with 1000 mm flow cells was employed. The setup was
243   designed to analyze four channels: total oxidized nitrogen (TON), silicate, nitrite, and phosphate,
244   using methods outlined in QuAAtro Applications: Method Nos. Q-068-05 Rev. 11, Q-066-05
245   Rev. 5, Q-070-05 Rev. 6, and Q-064-05 Rev. 8, respectively. To ensure analytical consistency
246   and validate the data, each run was checked against Certified Reference Material for Nutrients in
247   Seawater (RMNS). Nutrient analyses were further validated using KANSO CRM, with specific
248   lot numbers for macromolar and nanomolar nutrient concentrations.

Figure 3. Underway pH drift correction using $pH_{total(TA/DIC)}$ subsamples for a) cruise SO279 and b) cruise SO289. Raw pH measurements (pink); corrected pH values and uncertainty from bootstrapping (blue); subsample $pH_{total(TA/DIC)}$ depicted as black circles.

2.5 Post-cruise correction

253

254 To ensure the reliability of the dataset, an initial screening was conducted to identify and flag
255 unreliable continuous pH data points, primarily attributable to optode stabilization issues.
256 Specifically, data points exhibiting unreasonable drift patterns, inconsistent with expected optode
257 and surface ocean pH behavior, were flagged as unreliable.

258

259 $pH_{TA, DIC}$ values were calculated from TA and DIC UWS discrete samples and were then aligned
260 with the continuous pH data to calculate the offset between the $pH_{TA, DIC}$ subsamples and the
261 continuous pH data (Fig. 3). A Piecewise Cubic Hermite Interpolating Polynomial (PCHIP;
262 (Fritsch & Carlson, 1980) was fitted to the offset as a way to continuously correct pH variations
263 across the entire pH timeseries (Fig. 3).

2.6 Estimation of other biogeochemical parameters

264

265 TA was estimated for the continuous pH dataset using the empirical equations presented by Lee
266 et al. (2006). For the North Atlantic, the corresponding equation was used (see Fig. S1 in
267 supplementary information):

268

$$TA_{NA} = 2305 + 53.97(SSS - 35) + 2.74(SSS - 35)^2 - 1.16(SST - 20) \atop + 0.040(SST - 20)^2 \tag{1}$$

269 In contrast, the (Sub)tropics equation (SBT, Eq. 2) was applied for the South Pacific region, as
270 the cruise mostly followed the 32.5°S longitude and this equation was determined to offer the
271 best fit to the local temperature (SST) and salinity (SSS) equation (see Fig. S1 in supplementary
272 information):

273

$$TA_{SBT} = 2305 + 58.66(SSS - 35) + 2.32(SSS - 35)^2 - 1.41(SST - 20) \atop + 0.040(SST - 20)^2 \tag{2}$$

274

275 TA estimates were used together with pH to solve the rest of the marine carbonate system (i.e.
276 DIC and fCO_2) using PyCO2SYS (Version 1.8.2; (Humphreys et al., 2022), with the carbonic
277 acid dissociation constants of Sulpis et al. (2020), the bisulfate dissociation constant of Dickson
278 (1990), the total boron to chlorinity ratio of Uppström (1974), and the hydrogen fluoride
279 dissociation constant of Dickson and Riley (1979).

2.7 Projected pH variability

280

281 The derived parameters pH_{temp}, pH_{sal}, and $pH_{temp,sal}$ were calculated while holding TA and DIC
282 constant at the average values of each diurnal cycle. These calculations allowed for the
283 exploration of changes in pH under varying environmental conditions by solely altering either
284 temperature, salinity, or both simultaneously. $pH_{TA, fCO2}$ was also computed while holding TA
285 and fCO_2 constant at their daily mean values but with varying temperature and salinity to model
286 the pH distribution under fully equilibrated conditions. All calculations were done using the
287 same options in PyCO2SYS described in Sect. 2.6.

2.8 Identification of full diurnal cycles

To account for the influence of geographic location on temporal measurements, timestamps from Coordinated Universal Time (UTC) were converted to Local Solar Time (LST). This conversion was necessary to align time-sensitive data with the true solar position at each measurement location, thereby facilitating more accurate comparisons of environmental data across different geographic regions and improving the analysis of diurnal processes.

The conversion process involved calculating the mean longitudinal position for each date within the dataset. Subsequently, a time offset was determined based on the average longitude, assuming a standard rate of Earth's rotation. This offset was then applied to the original UTC timestamps, resulting in a modified dataset with timestamps adjusted to reflect LST:

$$\text{DateTime}_{\text{LST}} = \text{DateTime}_{\text{UTC}} + \left(\frac{\text{Longitude}_{\text{mean}}}{15}\right). \tag{3}$$

Following the conversion to LST, the dataset was further processed to isolate complete diurnal cycles to ensure that only data representing full 24-hour cycles were included. The North Atlantic dataset included 7 complete diurnal cycles, while the South Pacific dataset included 11 complete diurnal cycles.

2.9 Uncertainty propagation

2.9.1 Uncertainty in pH measurements and post-correction

The final uncertainty in pH measurements was estimated by combining uncertainties from two main sources: (1) the uncertainty in the TA and DIC measurements used to calculate $pH_{(TA/DIC}$ and (2) the correction of the UWS pH measurements using $pH_{TA, DIC}$.

First, the precision in TA and DIC were determined based on the RMSE from repeated measurements of a known standard water sample in the laboratory (NIOZ; 0.92 umol/kg and 1.95 µmol/kg, respectively). Then a Monte Carlo simulation was applied to the calculated $pH_{TA, DIC}$ to obtain a pH_{RMSE} for each subsample $pH_{TA, DIC}$.

Next, the pH measurements obtained from the optode were corrected using $pH_{(TA, DIC)}$ from the discrete measurements of TA and DIC. The uncertainty in the pH correction was assessed using a bootstrapping approach (n=1000 iterations), where a fraction (50%) of the discrete samples was randomly omitted in each iteration and the selected fraction of the discrete samples varied within its own pH_{RMSE}.

The variation in each subsample's $pH_{TA, DIC}$ captured the likely variability in TA and DIC measurements, while omitting different subsets of data allowed for the estimation of how sensitive the pH correction is to which set of subsamples are used for calibration.

2.9.2 Uncertainty in pH diurnal patterns

To ensure the observed patterns in pH over the full 24-hour cycles were not artifacts of sampling bias or other anomalies, a Monte Carlo simulation (n = 1000 iterations) was employed on each diurnal cycle's hourly data analysis. This simulation randomly selected 50% of the data points for

328   each hour (i.e. 50% of 120 hourly measurements for the North Atlantic dataset and 50% of 240
329   hourly measurements for the South Pacific dataset), repeatedly calculating the mean pH to assess
330   the consistency and robustness of the hourly trends. This component of the uncertainty proved
331   insignificant (i.e., errors bars were smaller than the symbols in Fig. 4 and 5).

332   **2.10 CO$_2$ air-sea flux dynamics**

333   The difference in pCO$_2$ between the air and ocean surface dictates the direction of gas exchange
334   and determines whether the ocean acts as a CO$_2$ source or sink to the atmosphere. This CO$_2$
335   exchange between the air and sea, referred to as CO$_2$ flux, can be computed based on the
336   relationship:
337

$$F = k_{\mathrm{w}} \times K_0 \times (pCO_{2_{\mathrm{sw}}} - pCO_{2_{\mathrm{air}}}) \tag{4}$$

338
339   where F represents the flux of CO$_2$ across the air-sea interface, k_{w} is the gas transfer velocity,
340   K_0 is the solubility constant and $pCO_{2_{\mathrm{sw}}}$ is the partial pressure of CO$_2$ in sea water, representing
341   the concentration of dissolved CO$_2$ that is in equilibrium with the atmosphere and $pCO_{2_{\mathrm{air}}}$ is the
342   partial pressure of CO$_2$ in the atmosphere above the ocean surface. For the fluxes, a positive
343   value shows the ocean acts as a source (i.e., releasing CO$_2$ to the atmosphere), while a negative
344   value shows it acts as a sink (i.e., absorbing CO$_2$ from the atmosphere). The parameterisation
345   from Ho et al. (2006) was used to determine the gas transfer velocity. All fluxes were computed
346   using the pySeaFlux package (v2.2.2; (Fay et al., 2021).
347
348   Flux calculations were performed for each complete diurnal cycle, followed by the computation
349   of the mean flux for each cycle. Additionally, the mean flux for the diurnal cycle was also
350   calculated from the daily mean inputs (wind speed, temperature, salinity, and pCO$_2$), and
351   specifically computed for the hours 12 AM and 12 PM (LST) to examine temporal variations
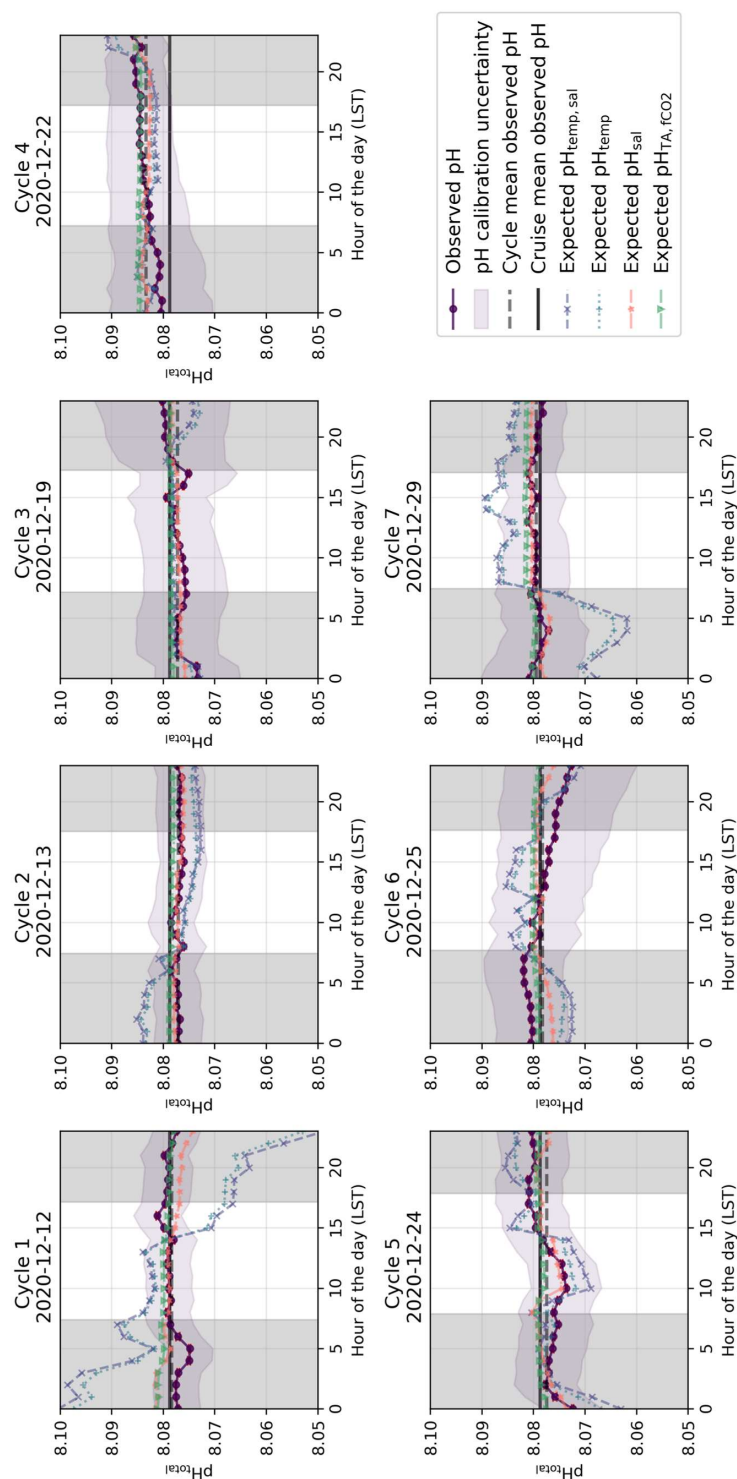352   within each cycle.

Figure 4. Identified diurnal cycles for cruise SO279 in the North Atlantic Ocean. Dark purple lines show observed pH, dashed grey lines show mean observed pH over the full diurnal cycle, and black lines show overall mean pH for all diurnal cycles combined for that cruise. The remaining shows expected pH using constant TA and DIC (averaged for each respective diurnal cycle) and varying temperature and salinity (dashed light purple lines), varying temperature alone (dashed blue lines), varying salinity alone (dashed orange lines) and constant TA and fCO$_2$ (dashed green lines). Grey areas are night hours.
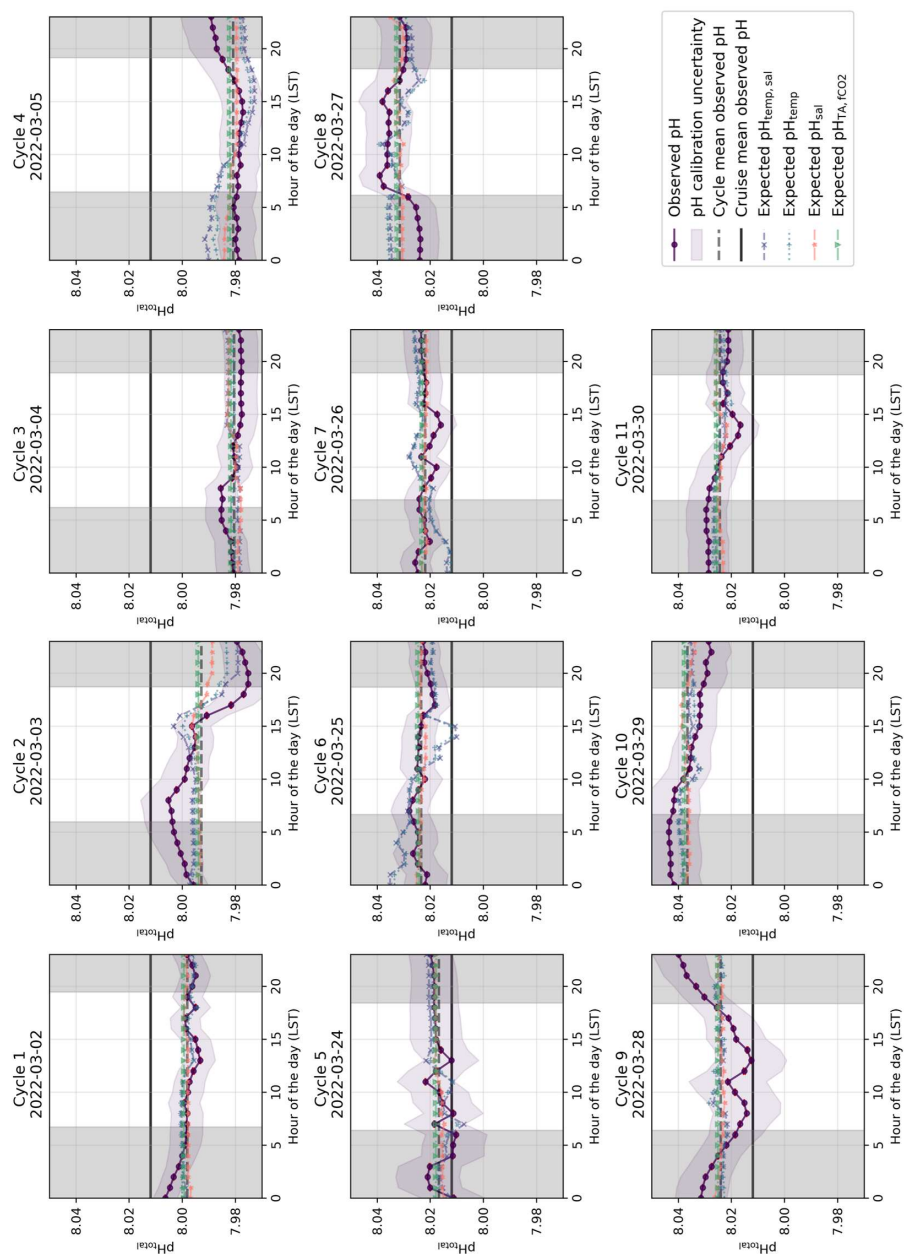
353

354

Figure 5. Identified diurnal cycles for cruise SO289 in the South Pacific Ocean. Dark purple lines show observed pH, dashed grey lines show mean observed pH over the full diurnal cycle, and black lines show overall mean pH for all diurnal cycles combined for that cruise. The remaining shows expected pH using constant TA and DIC (averaged for each respective diurnal cycle) and varying temperature and salinity (dashed light purple lines), varying temperature alone (dashed blue lines), varying salinity alone (dashed orange lines) and constant TA and fCO2 (dashed green lines). Grey areas are night hours.
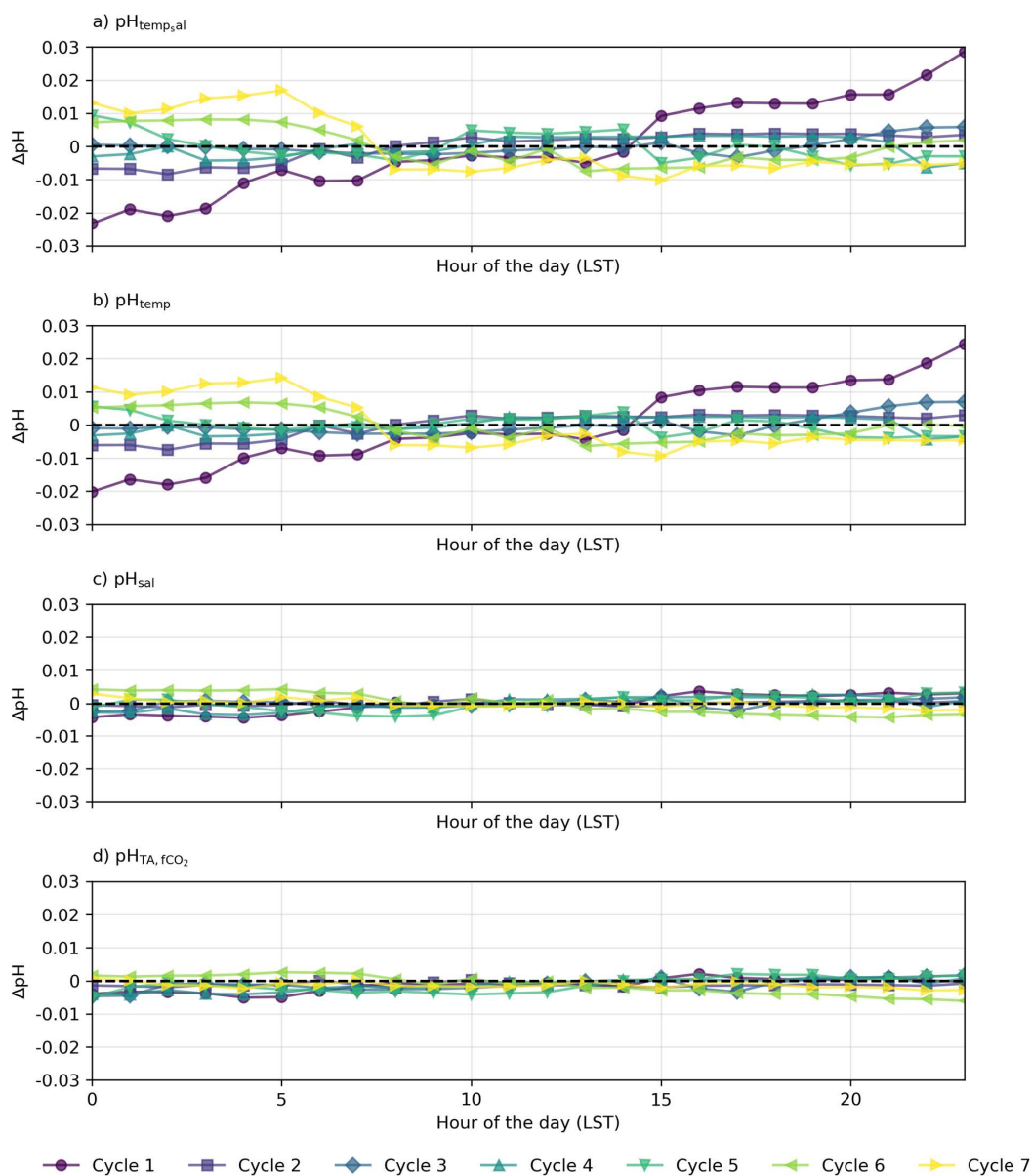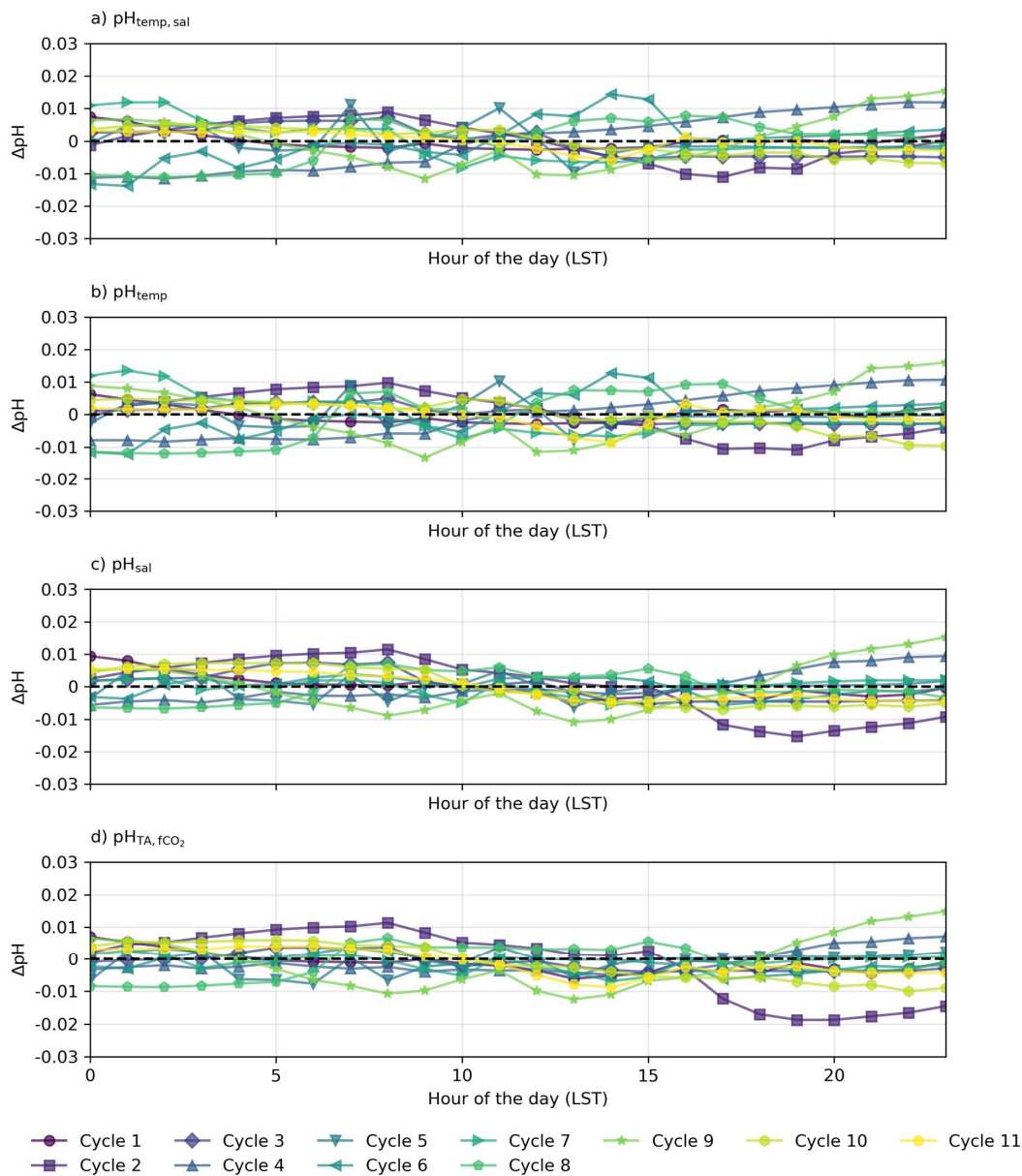
Figure 6. Residual plots for diurnal cycles in the North Atlantic, illustrating the discrepancies between observed pH measured by the optode (pH$_{obs}$) and a) pH calculated from constant TA and DIC with varying temperature and salinity (pH$_{temp,sal}$), b) varying temperature only (pH$_{temp}$), c) varying salinity only (pH$_{sal}$) and d) constant TA and fCO$_2$ with varying temperature and salinity . Horizontal dashed lines at y=0 indicate no deviation between observed and calculated pH.

362

363
364
365 **Figure 7. Residual plots for diurnal cycles in the South Pacific, illustrating the discrepancies between**
366 **observed pH measured by the optode (pH$_{obs}$) and a) pH calculated from constant TA and DIC with varying**
367 **temperature and salinity (pH$_{temp,sal}$), b) varying temperature only (pH$_{temp}$), c) varying salinity only (pH$_{sal}$) and**
368 **d) constant TA and fCO$_2$ with varying temperature and salinity . Horizontal dashed lines at y=0 indicate no**
369 **deviation between observed and calculated pH.**

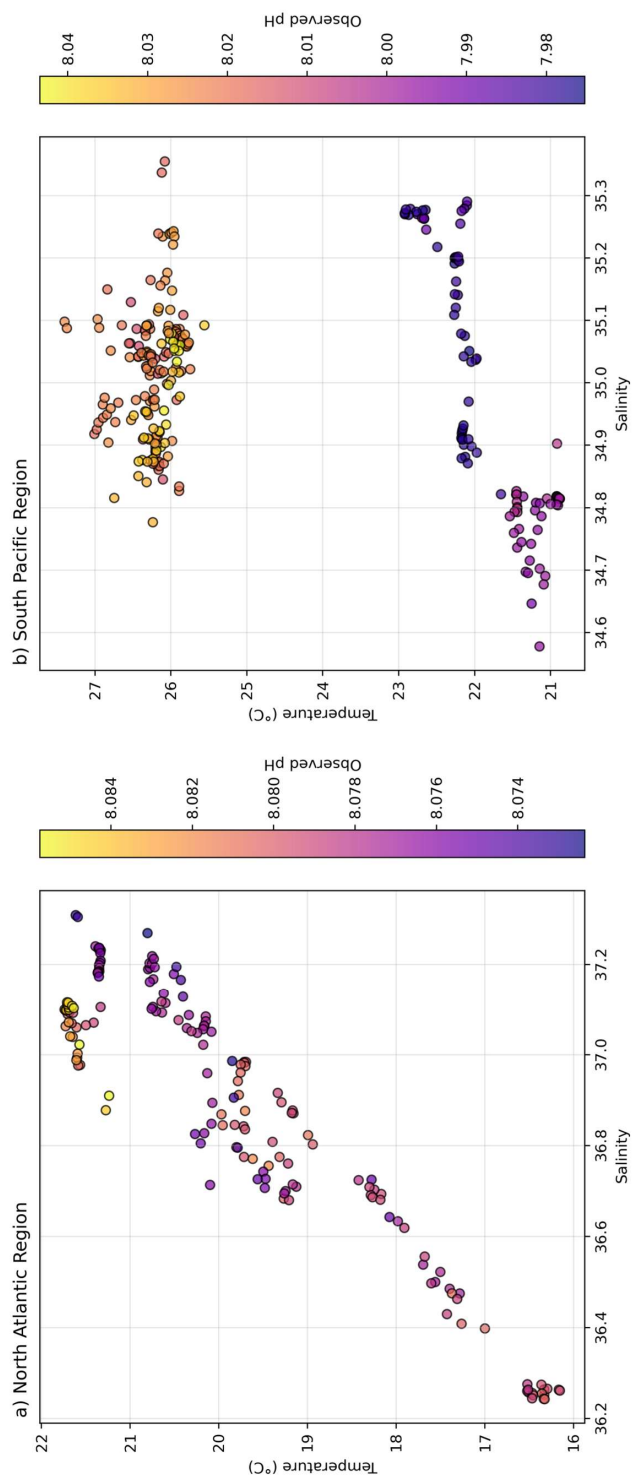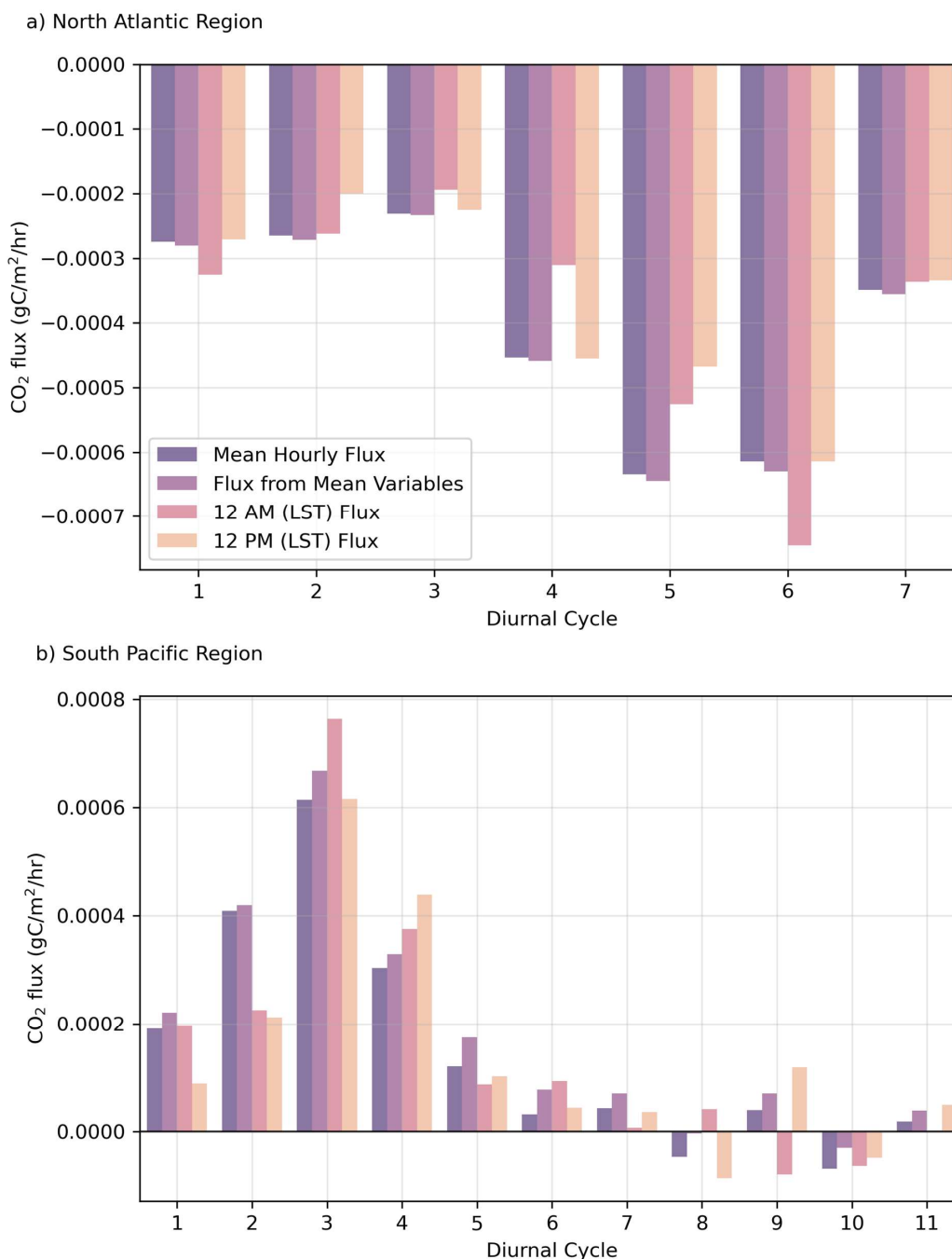**Figure 8. T/S diagram with observed pH for a) the North Atlantic region and b) the South Pacific region.**

Figure 9. Sensitivity analysis of mean CO₂ flux compared to flux calculated from mean inputs, fluxes for 12 AM (LST) and fluxes for 12 PM (LST). Top panel a) shows cruise SO279 in the North Atlantic while bottom panel b) shows cruise SO289 in the South Pacific.

3 Results and Discussion

375

376 We first analyse the effects of temperature and salinity on pH across different diurnal cycles and
377 regions (Sect. 3.1). We examine the pH expected from temperature and salinity variations alone
378 ($pH_{temp,sal}$), disregarding changes in TA or DIC. If pH_{obs} aligns with $pH_{temp,sal}$, it suggests that
379 recent temperature changes, such as day-night cycles, primarily control pH. In this context,
380 "recent" is relative to the air-sea CO_2 equilibration timescale, i.e., temperature change that
381 happened recently enough that its effect on pH has not been modified by subsequent gas
382 exchange. Next, we assess the influence of water mass variations on pH by considering
383 $pH_{TA,fCO2}$, which accounts for constant fCO_2 instead of DIC alongside constant TA and varying
384 temperature and salinity. Alignment of pH_{obs} with $pH_{TA,fCO2}$ indicates that slower or long-ago
385 processes control pH. For example, an observed change in temperature may be due to spatial
386 variability, with the ship passing through different water masses that have had different
387 temperatures for long enough to reequilibrate with atmospheric CO_2. We then explore the role of
388 biological activity and its interaction with abiotic factors by looking at the discrepancies between
389 pH_{obs} and both $pH_{temp,sal}$ and $pH_{TA,fCO2}$ (Sect. 3.2). Finally, we distinguish between temporal and
390 spatial variability in our measurements (Sect. 3.3), considering implications for air-sea CO_2
391 equilibration timescales at fine spatio-temporal scales (Sect. 3.4).

3.1 Influence of temperature and salinity

392

393 The diurnal cycles of pH observed in the North Atlantic and South Pacific Oceans are
394 significantly influenced by temperature. In most cycles, observed pH stays within ±0.01 of
395 $pH_{temp,sal}$ thus indicating that temperature and salinity together drive pH changes (Fig. 6 and 7).
396 However, salinity alone does not appear to strongly influence pH in any observed cycle. For both
397 ocean basins, pH_{sal} typically remains close to the mean pH of each cycle, rather than impacting
398 the observed pH significantly. This consistency suggests that daily salinity variations do not
399 exert a primary influence on the observed pH (Fig. 4 and 5; Fig. 6c; Fig. 7c). Thus, the rest of
400 this section focuses on the effect of temperature on the observed pH.
401

402 On short timescales (minutes and faster), temperature influences pH by affecting the dissociation
403 of carbonic acid (H_2CO_3) into bicarbonate (HCO_3^-) and carbonate (CO_3^{2-}) ions. As temperature
404 changes, the dissociation constants of carbonic acid change, which in turn alters the
405 concentrations of these ions and the overall pH of the solution. This dependency shifts the
406 equilibrium of these species with changing temperature and affects pH over short timescales (i.e.,
407 seconds to minutes; (Egleston et al., 2010; Stumm & Morgan, 2012). However, the overall
408 response can be lessened by the stabilizing effect of alkalinity, which keeps the pH steady
409 despite temperature changes (Frankignoulle, 1994; Middelburg et al., 2020). The alkalinity of
410 seawater allows the carbonate system and other weak acid-base equilibria to maintain pH by
411 absorbing or releasing protons, which reduces the impact of temperature changes on pH
412 (Dickson & Millero, 1987; Egleston et al., 2010). Typically, the most pronounced temperature
413 fluctuations—highest temperatures during daylight and lowest at night—occur in surface waters.
414 This is due to surface waters' lower thermal inertia and direct exposure to the atmosphere. In
415 contrast, deeper waters have a smaller thermal response because they are insulated from direct
416 atmospheric influence and have a higher heat capacity, which buffers them against rapid
417 temperature changes.
418

419   In the North Atlantic, the observed variability in pH generally matches the calculated pH_{temp} and
420    $pH_{temp,sal}$, with most cycles' residuals within ±0.01 (Fig. 4 and Fig. 6a and b, Cycles 2, 3, 4, 5 and
421   6). However, some cycles match better than others. Cycle 3 demonstrates a consistent alignment
422   between observed pH and expected $pH_{temp,sal}$ throughout the day, with minimal oscillations
423   around the mean (mean residuals for $pH_{temp,sal}$ of less than -0.001; Fig. 4; Fig. 6a and b). A
424   similar pattern is observed in Cycle 4, where pH variations are minimal (residuals range from -
425   0.007 to 0.003 for $pH_{temp,sal}$, with a mean of less than -0.001; Fig. 4). In contrast, in Cycle 5,
426   pH_{obs} and $pH_{temp,sal}$ show close agreement throughout the day with residuals close to zero,
427   indicating a stable match despite slight deviations from that day's cycle mean. Cycle 6 also
428   displays more pronounced daily fluctuations in pH_{temp} and $pH_{temp,sal}$ with residuals from -0.008 to
429   +0.008 (Fig. 6) but that still closely follow pH_{obs} (within the ±0.01 residuals; Fig. 4). In the South
430   Pacific, similar patterns are evident in Cycles 1, 3, 4, and 6, with consistent and minimal
431   fluctuations around the cycle mean (Fig. 5). Cycle 3 in particular shows most stability, with all
432   expected pH values remaining within a narrow range of the observed pH (i.e. mean residuals for
433    $pH_{temp,sal}$ of less than 0.001; Fig. 5; Fig. 7a and b). Similarly, in Cycles 4, 10 and 11, pH_{obs}
434   closely match $pH_{temp,sal}$ across the day, and exhibit minimal residuals (< 0.01; Fig. 5 and 7a and
435   b).

437   However, notable discrepancies occur in pH observations versus calculated pH_{temp} and $pH_{temp,sal}$
438   in the North Atlantic. Specifically, in Cycle 1, while pH_{obs} remains relatively stable, there are
439   significant daily fluctuations in pH_{temp} and $pH_{temp,sal}$, with residuals ranging from -0.023 to 0.029
440   and a mean of less than -0.001 (Fig. 4; Fig. 6a, b, and c). Cycles 5 and 7 also show discrepancies:
441   although pH_{obs} generally matches the cruise mean across all cycles, $pH_{temp,sal}$ exhibits greater
442   deviations, indicating that some other process has eliminated the temperature signal in the
443   observed pH (Fig. 4; Fig. 6a and b). In the South Pacific, similar patterns emerge. Cycle 5 shows
444   significant hourly fluctuations in pH_{obs}, which closely track the deviations in pH_{temp} and
445    $pH_{temp,sal}$, markedly diverging from the more stable pH_{sal} (Fig. 5; Fig. 7a and b). Additionally, in
446   Cycle 2, the initial excess and subsequent shortfall in pH_{temp} and $pH_{temp,sal}$, with residuals from -
447   0.011 to 0.008, suggest a comparable moderated effect by solar heating (Fig. 4). This pattern is
448   consistent with observations in the North Atlantic. This overriding influence, likely due to solar
449   heating, impacts the diurnal pH fluctuation patterns, particularly in cycles where pH_{temp} and
450    $pH_{temp,sal}$ start higher and decrease throughout the day.

452   While changes in pH and fCO_2 due to temperature change occur virtually instantaneously (i.e.,
453   seconds to minutes), CO_2 equilibration between the atmosphere and the ocean is considerably
454   slower (i.e., weeks to months; Jones et al. (2014). This means that the timescale of temperature
455   change significantly influences how a water masses' pH adjusts to temperature changes
456   (Takahashi et al., 2009). For instance, when a water mass cools during the night, it quickly alters
457   pH and causes CO_2 undersaturation due to increased solubility, so observed pH would agree with
458   pH_{temp} (Feely et al., 2008). However, as the ship travels through different water masses that vary
459   in temperature, but are each in equilibrium with the atmosphere, observed pH may not align with
460   pH_{temp} or $pH_{temp,sal}$ calculated based on temperature shifts alone. This raises an issue regarding
461   the timescales of temperature change in relation to chemical equilibration, as it is uncertain
462   whether these changes provide the system enough time for fCO_2 (and DIC) to shift and maintain
463   equilibrium with the atmosphere, or if they happen more rapidly, such that disequilibrium
464   remains.

465

466 In the North Atlantic, significant mixing due to ocean currents, eddies, and upwelling introduces
467 substantial variability in temperature, salinity, and pH across different water masses (Fig. 6a and
468 b). This variability is further influenced by the Gulf Stream and North Atlantic Drift, which
469 create complex structures of distinct water masses (Liu & Tanhua, 2021). These dynamic
470 conditions adjust the rate of CO_2 absorption or release, impacting the timescale over which
471 ocean-atmosphere equilibrium is achieved. But in this ocean basin, $pH_{TA,fCO2}$ (i.e. proxy for gas-
472 exchange equilibrium) follows pH_{obs} very closely, indicating that temperature changes have been
473 sufficient for the system to reach re-equilibration. This is true both for individual cycles' diurnal
474 distributions (Fig. 4), and when comparing the cycles' residuals together, which are virtually
475 zero (Fig. 6d), even during temperature gradient crossings (Fig. S4).

476

477 In contrast, the South Pacific displays more predictable water mass dynamics primarily driven by
478 physical processes like mixing and advection, which introduce water masses with consistent
479 temperatures, salinities, and pH, resulting in a more homogeneous water column. This stability is
480 influenced by large-scale gyres and trade winds, contributing to the uniformity of surface waters
481 (Vallis, 2017). This is reflected by the consistent pH_{obs}. Residuals are further from zero although
482 most cycles fall within ±0.01, indicating a lesser degree of re-equilibration (Fig. 7).

483

484 Thus, this implies that, in both ocean basins, gas exchange plays a significant role in stabilizing
485 pH for all cycles by re-equilibrating with atmospheric CO_2 despite temperature fluctuations –
486 although it likely does more so in the North Atlantic than in the South Pacific. To first order, this
487 also suggests that the temperature change happened long enough ago for re-equilibration.
488 However, the rates of gas exchange in the North Atlantic and South Pacific are from 3 to 6
489 months and 3 to 4 months, respectively (Jones et al., 2014). Thus, the consistency between
490 $pH_{TA,fCO2}$ and pH_{obs} likely represents the crossings of water masses that are in equilibrium with
491 the atmosphere and that equilibrated a long time ago (i.e., weeks to months) with different TA,
492 DIC, and temperature baselines. Thus, the observed temperature changes as the ship traverses
493 different water masses are likely attributable to spatial variations rather than an immediate
494 response to recent temperature shifts. However, some pH cycles observed do not fully conform
495 to these patterns, suggesting that other factors could be influencing the pH beyond the effects of
496 temperature and gas exchange alone.

497

498 Ultimately, although we observe temperature-induced variations throughout each diurnal cycle,
499 when comparing all cycles' pH_{obs}, pH_{temp} and $pH_{temp,sal}$ within both ocean basins, residuals are
500 well within ±0.02 (Fig. 6a and b and Fig. 7a and b). Thus, despite observed 24-hour fluctuations,
501 pH remains relatively stable with respect to temperature variations across both ocean basins. This
502 stability implies that even though there are short-term fluctuations in pH due to temperature
503 changes, overall the pH stays relatively consistent, and thus a stable ocean-atmosphere CO_2
504 equilibrium.

505 **3.2 Influence of biological activity**

506 While temperature and salinity effects on pH have been addressed in Sect. 3.1, deviations from
507 expected patterns may be shaped by biological processes. The process of photosynthesis during
508 daylight consumes CO_2, leading to a rise in pH, whereas respiration and decomposition at night,
509 which release CO_2, lower pH (Falkowski, 1994; Falkowski & Raven, 2013). The balance

510   between photosynthesis and respiration hence affects pH, and should result in a diurnal pH cycle.
511   These biological processes can also influence the rate at which CO_2 equilibrates between the
512   ocean and atmosphere. For instance, intense photosynthetic activity during daylight hours can
513   rapidly deplete seawater pCO_2 in surface waters, potentially accelerating seawater CO_2 uptake
514   from the atmosphere. Conversely, nighttime respiration can increase pCO_2, slowing the
515   outgassing process and thus extending the equilibration timescale. However, given an
516   equilibration timescale of months, these day and night changes likely get averaged out over
517   longer periods, resulting in an overall steady-state CO_2 flux and pH when observed over longer
518   temporal scales.
519
520   These biological processes are particularly evident in some cycles from the North Atlantic where
521   the expected $pH_{temp,sal}$ changes due to temperature and salinity do not align with the observed
522   data, but do follow the distribution expected from biological activity (Fig. 4). This is especially
523   evident for Cycle 1, which shows an increase in pH during daylight hours and a decrease in pH
524   during night hours, with a peak in pH in late afternoon and the lowest pH occurring in the early
525   morning before sunrise (Fig. 4). Other cycles likely reflect the combined impact of biological
526   processes and temperature effects, as the observed pH does not fully align with the distribution
527   expected from any of temperature, salinity or biological activity (Fig. 4 and 6). This is also
528   evident in the South Pacific Ocean, where some cycles show significant variability within pH_{obs}
529   that are not mirrored by the expected $pH_{temp,sal}$ changes (Fig. 5, Cycles 2, 8). For example, Cycle
530   2 exhibits significant deviations in pH with higher observed values in the morning and a drop in
531   the afternoon, indicating biological influence (Fig. 5).
532
533   The interplay between photosynthesis during the day and respiration at night, with possible
534   contributions of other biological processes, may be behind the more pronounced peaks and
535   troughs of Cycles 2 and 9 (Fig. 6; Duarte and Agusti (1998). Nitrogen fixation consumes
536   hydrogen ions, increasing pH, whereas denitrification releases hydrogen ions, thereby decreasing
537   pH (Richardson, 2000; Zehr & Kudela, 2011). However, without nutrient and oxygen data, we
538   cannot directly assess whether these processes also impacted the observed pH.
539
540   Although biological activity likely accounts for some variability, not all cycles exhibit the same
541   residual, presumably biotic pattern of variation (Fig. 4 and 5). This variability further
542   complicates assessments of air-sea CO_2 equilibration, as localized biological conditions may
543   transiently alter CO_2 dynamics, influencing the timescale for reaching equilibrium. This is more
544   obvious in the South Pacific, where some cycles display more pronounced night-time stability
545   (Fig. 5, Cycles 3, 6, 7 and 11), while others have noticeable day-time fluctuations that could
546   align with photosynthetic activity, which typically increase during daylight hours (Fig. 5, Cycle
547   8; (Duarte & Agusti, 1998; Raven & Johnston, 1991). Cycle 8 in the South Pacific shows a peak
548   in observed pH around midday, likely due to increased photosynthesis, followed by a decrease in
549   the evening (Fig. 5). Other cycles do not show this pattern as clearly (i.e., they even show a
550   decrease of pH during the day), suggesting that, for some cycles, respiration may dominate over
551   photosynthesis also during daytime (Fig. 5). For example, Cycle 9 displays significant variations
552   in pH throughout the day, with notable decreases during daylight hours (Fig. 5). Additionally, as
553   some cycles appear to conform to temperature-based pH expectations, the only minor deviations
554   observed suggest biological activity to be minor or represent a balanced biological system where
555   photosynthesis and respiration are in near-equilibrium (Fig. 5, Cycles 3 and 6).

556

557 Despite the strong impact of both abiotic and biotic factors on pH, some cycles exhibit fine-scale
558 trends that cannot be solely attributed to temperature fluctuations or biological activity. The fine-
559 scale trends observed, especially in Cycles 1 and 7 (Fig. 4), exceed what can be attributed to
560 temperature-induced changes alone and cannot be explained by biological activity, given the
561 atypically high carbon fixation rates required to explain the pH offsets (Basu & Mackey, 2018;
562 Wang et al., 2023). Indeed, the required biological carbon fixation would need to exceed 687 mg
563 C m^3 day to explain the offset (Text S7). Typical rates in open ocean waters are much lower,
564 generally ranging from 50 to 150 mg C m^3 day^{-1} in nutrient-poor regions and can reach up to
565 1000 C m^3 day^{-1} in upwelling zones during phytoplankton blooms, which is not the case here
566 (Basu & Mackey, 2018; Wang et al., 2023).

567

568 Comparing the impact of biological activity based on the offsets between pH$_{temp}$ and pH$_{obs}$ with
569 chlorophyll-a fluorescence data also shows no clear pattern (Fig. S2 and S3). This is expected as
570 fluorescence does not necessarily reflect instantaneous photosynthetic activity. Instead,
571 fluorescence primarily indicates the presence and abundance of phytoplankton. Therefore, while
572 fluorescence can provide insights into the overall biomass of phytoplankton, it does not directly
573 correlate with photosynthesis and respiration. The absence of a clear correlation between
574 fluorescence and the daily pH cycle, with some cycles even showing a decrease in pH during
575 daytime, confirms that the influence of different water masses is important in shaping the local
576 high-resolution pH profiles.

577 **3.3 Variability and stability in spatio-temporal pH patterns**

578 The North Atlantic is characterized by complex interactions among water masses, leading to
579 higher turbulence and susceptibility to rapid and significant changes in water mass properties and
580 circulation patterns, influenced by both past and present climatic conditions (Lynch-Stieglitz,
581 2017; Gebbie, 2014). This complexity is partly due to the Atlantic Meridional Overturning
582 Circulation (AMOC), which is sensitive to various climate perturbations and has historically
583 undergone significant reorganizations, especially during climatic transitions such as the Last
584 Glacial Maximum (Curry and Oppo, 2005; Duplessy et al., 1988). As examined in Sect. 3.1,
585 considerable spatial variability is observed in the North Atlantic (Fig. 8 and Fig. S6), and this
586 heterogeneity introduces complexity in deciphering the relative contributions of abiotic and
587 biotic factors to pH fluctuations (Gruber & Sarmiento, 2002). Residual plots for the North
588 Atlantic suggest that the observed discrepancies between pH$_{obs}$ and both pH$_{temp}$ and pH$_{temp,sal}$ are
589 insignificant, indicating that variability in water mass characteristics—which include but are not
590 limited solely to temperature and salinity—do not dominate the observed pH variability (Fig. 6
591 and 8). Therefore, the hourly fluctuations in pH$_{obs}$ and the observed discrepancies between pH$_{obs}$
592 and pH$_{temp/sal}$ across various cycles in this ocean basin may not be attributed to pronounced
593 spatial variability (Fig. 4). The T/S diagram also demonstrates this spatial variability, showing a
594 wide range of pH values correlated with differing salinity and temperature profiles across various
595 water masses (Fig. 8), reinforcing that spatial dynamics do not significantly influence pH
596 variation in this region. This is also supported by the relative stability observed in Cycle 4, where
597 the ship's consistent positioning (i.e. on station) highlights the role of temporal variability rather
598 than spatial variability (Fig. S4). Although water could still be moving spatially around the ship,
599 the variability could be due to some degree to different water masses rather than being limited to
600 true in-situ temporal variability.

601

602   In contrast, the South Pacific cruise predominantly exhibits a stable transit through more
603   homogeneous surface waters as no SST gradient is observed, although it is not entirely free from
604   disruptions (Fig. 8 and Fig. S5; Qu and Lindstrom (2004). This suggests a minor role of
605   interactions between diverse water masses. Despite the hourly fluctuations observed, all diurnal
606   cycles in the South Pacific tend to cluster closely around the mean pH for their respective 24-
607   hour periods, reflecting substantial stability within each cycle but considerable variability across
608   different days, particularly evident among consecutive cycles (Fig. 5). This underscores a clear
609   temporal delineation of diurnal cycles influenced by DIC changes (Fig. 5).

610   **3.4 Implications for air-sea CO_2 fluxes**

611   Our findings indicate that while temperature and salinity predominantly govern diurnal pH
612   fluctuations, additional variability arises from water mass dynamics and biological activity.
613   Temperature rapidly affects pH, but the slower rate of CO_2 equilibration with the atmosphere
614   moderates its impact on air-sea CO_2 fluxes. Although biological processes markedly influence
615   daily pH cycles, they do not fully account for the observed variability, especially in cases where
616   unusually high carbon fixation rates would be required to explain observed pH (Sect. 3.2).

617

618   CO_2 fluxes were calculated for each complete diurnal cycle (Fig. 9). The flux calculations were
619   performed by computing the mean flux for each cycle from daily mean inputs (wind speed,
620   temperature, salinity, and pCO$_2$) and specifically for the hours 12 AM and 12 PM (LST) to
621   examine temporal variations within each cycle (Fig. 9). Despite different methods of calculation,
622   the CO_2 fluxes remained relatively consistent, indicating that the variations in pH and thus CO_2
623   flux do not significantly affect the air-sea CO_2 exchange in either basin.

624

625   This consistent result shows that despite the processes influencing pH in these two ocean basins
626   during the study period, the surface ocean's interaction with atmospheric CO_2 over longer
627   timescales (eg. months) can minimize the effect on pH, leading to relatively low variability on
628   short spatiotemporal scales (kilometers/days).

629   **4. Conclusions**

630   High-resolution pH data is crucial for understanding the subtle yet important variations in ocean
631   surface water pH across different regions. Diurnal cycles and hourly fluctuations in pH, with
632   varying magnitudes, can be observed in both the North Atlantic and South Pacific basins.
633   Variability in pH is influenced not only by temperature but also by interactions between various
634   water masses and biological activity. These factors together drive observed pH fluctuations,
635   often diverging from predictions based solely on temperature. However, although the processes
636   responsible for these pH variations are well-understood, high-resolution data highlight the
637   challenge of identifying a dominant factor at the fine-scale due to their complex interplay.

638

639   In both the North Atlantic and South Pacific, the close correlation between $pH_{TA,f\text{CO}2}$ and
640   observed pH across diurnal cycles suggests a significant role of gas exchange in stabilising pH
641   despite temperature fluctuations. The temperature changes must therefore have happened more
642   slowly than the air-sea CO_2 equilibration timescales for these ocean basins. The observed,
643   relatively constant pH is likely due to the ship passing through different water masses that had
644   already equilibrated with the atmosphere.

645

646 Thus, despite short-term fluctuations in pH, there were no major changes in ocean-atmosphere
647 CO_2 disequilibrium, indicating that, for the regions and time periods studied here, broader ocean-
648 basin scale analyses based on lower resolution datasets would still be able to capture the
649 necessary variability in surface ocean CO_2 chemistry for accurate global CO_2 cycle assessments.

650 *Data availability.* The hydrographic and biogeochemical data presented here, together with the
651 processing code will be freely available online at https://github.com/louisedelaigue/NA-SP-
652 HIGH-RES-PH by the time of publication.

653 *Supplement.* The supplement related to this article is available online.

654 *Author contributions*. LD and MPH conceptualized the project. CG, LD, MPH and YO curated
655 the data. LD, MPH and GJR performed the investigation. LD conceptualized the methodology,
656 used the necessary software, visualized the data and prepared the original draft of the paper. LD,
657 GJR, MPH, YO and CG reviewed and edited the paper.

658 *Competing interests.* The contact author has declared that neither they nor their co-authors have
659 any competing interests.

660 *Disclaimer.* Publisher's note: Copernicus Publications remains neutral with regard to
661 jurisdictional claims in published maps and institutional affiliations.

671 **References**

672 Achterberg, E. P., Steiner, Z., & Galley, C. G. (2022). South Pacific GEOTRACES Cruise No.
673 SO289, 18 February 2022–08 April 2022, Valparaiso (Chile)–Noumea (New Caledonia),
674 GEOTRACES GP21.
675 Basu, S., & Mackey, K. R. M. (2018). Phytoplankton as Key Mediators of the Biological Carbon
676 Pump: Their Responses to a Changing Climate. *Sustainability*, *10*(3), 869.
677 https://www.mdpi.com/2071-1050/10/3/869
678 Beck, A., Borchert, E., Delaigue, L., Deng, F., Gueroun, S., Hamm, T., Jacob, O., Kaandorp, M.,
679 Kokuhennadige, H., & Kossel, E. (2021). NAPTRAM-Plastiktransportmechanismen,
680 Senken und Interaktionen mit Biota im Nordatlantik/NAPTRAM-North Atlantic plastic
681 transport mechanisms, sinks, and interactions with biota, Cruise No. SO279, Emden
682 (Germany)–Emden (Germany), 04.12. 2020–05.01. 2021.

683 Caldeira, K., & Wickett, M. E. (2005). Ocean model predictions of chemistry changes from
684   carbon dioxide emissions to the atmosphere and ocean. *Journal of Geophysical Research:*
685   *Oceans*, *110*(C9).
686 Chavez, F. P., Sevadjian, J., Wahl, C., Friederich, J., & Friederich, G. E. (2018). Measurements
687   of pCO2 and pH from an autonomous surface vehicle in a coastal upwelling system.
688   *Deep Sea Research Part II: Topical Studies in Oceanography*, *151*, 137-146.
689   https://doi.org/https://doi.org/10.1016/j.dsr2.2017.01.001
690 Cornwall, C. E., Hepburn, C. D., McGraw, C. M., Currie, K. I., Pilditch, C. A., Hunter, K. A.,
691   Boyd, P. W., & Hurd, C. L. (2013). Diurnal fluctuations in seawater pH influence the
692   response of a calcifying macroalga to ocean acidification. *Proceedings of the Royal*
693   *Society B: Biological Sciences*, *280*(1772), 20132201.
694   https://doi.org/doi:10.1098/rspb.2013.2201
695 Cryer, S., Carvalho, F., Wood, T., Strong, J. A., Brown, P., Loucaides, S., Young, A., Sanders,
696   R., & Evans, C. (2020). Evaluating the Sensor-Equipped Autonomous Surface Vehicle C-
697   Worker 4 as a Tool for Identifying Coastal Ocean Acidification and Changes in
698   Carbonate Chemistry. *Journal of Marine Science and Engineering*, *8*(11), 939.
699   https://www.mdpi.com/2077-1312/8/11/939
700 Delaigue, L., Ourradi, Y., Bakker, K., Battermann, P., Galley, C., & Humphreys, M. P. (2023a).
701   *Discrete underway surface seawater dissolved inorganic carbon and total alkalinity for*
702   *R/V Sonne cruise SO289* Version V2) NIOZ. https://doi.org/doi:10.25850/nioz/7b.b.vf
703 Delaigue, L., Ourradi, Y., Bakker, K., Battermann, P., Galley, C., & Humphreys, M. P. (2023b).
704   *Underway surface seawater high-resolution pH time series for R/V Sonne cruise SO289*
705   Version V2) NIOZ. https://doi.org/doi:10.25850/nioz/7b.b.uf
706 Delaigue, L., Ourradi, Y., Ossebar, S., Battermann, P., Galley, C., & Humphreys, M. P. (2023).
707   *CTD seawater dissolved inorganic carbon and total alkalinity for R/V Sonne cruise*
708   *SO289* Version V6) NIOZ. https://doi.org/doi:10.25850/nioz/7b.b.tf
709 Delaigue, L., van Ooijen, J., & Humphreys, M. P. (2021a). *CTD seawater dissolved inorganic*
710   *carbon, total alkalinity and nutrients for R/V Sonne cruise SO279* Version V2) NIOZ.
711   https://doi.org/doi:10.25850/nioz/7b.b.kc
712 Delaigue, L., van Ooijen, J., & Humphreys, M. P. (2021b). *Discrete underway surface seawater*
713   *dissolved inorganic carbon, total alkalinity and nutrients for R/V Sonne cruise SO279*
714   Version V2) NIOZ. https://doi.org/doi:10.25850/nioz/7b.b.lc
715 Delaigue, L., van Ooijen, J., & Humphreys, M. P. (2021c). *Underway surface seawater high-*
716   *resolution pH time series for R/V Sonne cruise SO279* Version V2) NIOZ.
717   https://doi.org/doi:10.25850/nioz/7b.b.mc
718 DeVries, T. (2022). The Ocean Carbon Cycle. *Annual Review of Environment and Resources*,
719   *47*(1), 317-341. https://doi.org/10.1146/annurev-environ-120920-111307
720 Dickson, A., & Millero, F. J. (1987). A comparison of the equilibrium constants for the
721   dissociation of carbonic acid in seawater media. *Deep Sea Research Part A.*
722   *Oceanographic Research Papers*, *34*(10), 1733-1743.
723 Dickson, A. G. (1990). Standard potential of the reaction: AgCl(s) + 12H2(g) = Ag(s) + HCl(aq),
724   and and the standard acidity constant of the ion HSO4− in synthetic sea water from
725   273.15 to 318.15 K. *The Journal of Chemical Thermodynamics*, *22*(2), 113-127.
726   https://doi.org/https://doi.org/10.1016/0021-9614(90)90074-Z
727 Dickson, A. G., & Riley, J. P. (1979). The estimation of acid dissociation constants in sea-water
728   media from potentiometric titrations with strong base. II. The dissociation of phosphoric

729   acid. *Marine Chemistry*, *7*(2), 101-109. https://doi.org/https://doi.org/10.1016/0304-
730   4203(79)90002-1
731   Dickson, A. G., Sabine, C. L., & Christian, J. R. (2007). *Guide to best practices for ocean CO2*
732   *measurements*. North Pacific Marine Science Organization.
733   Doney, S. C., Busch, D. S., Cooley, S. R., & Kroeker, K. J. (2020). The Impacts of Ocean
734   Acidification on Marine Ecosystems and Reliant Human Communities. *Annual Review of*
735   *Environment and Resources*, *45*(Volume 45, 2020), 83-112.
736   https://doi.org/https://doi.org/10.1146/annurev-environ-012320-083019
737   Duarte, C. M., & Agusti, S. (1998). The CO2 balance of unproductive aquatic ecosystems.
738   *Science*, *281*(5374), 234-236. https://doi.org/10.1126/science.281.5374.234
739   Egea, L. G., Jiménez-Ramos, R., Hernández, I., Bouma, T. J., & Brun, F. G. (2018). Effects of
740   ocean acidification and hydrodynamic conditions on carbon metabolism and dissolved
741   organic carbon (DOC) fluxes in seagrass populations. *PLOS ONE*, *13*(2), e0192402.
742   https://doi.org/10.1371/journal.pone.0192402
743   Egilsdottir, H., Noisette, F., Noël, L. M. L. J., Olafsson, J., & Martin, S. (2013). Effects of pCO2
744   on physiology and skeletal mineralogy in a tidal pool coralline alga Corallina elongata.
745   *Marine Biology*, *160*(8), 2103-2112. https://doi.org/10.1007/s00227-012-2090-7
746   Egleston, E. S., Sabine, C. L., & Morel, F. M. (2010). Revelle revisited: Buffer factors that
747   quantify the response of ocean chemistry to changes in DIC and alkalinity. *Global*
748   *Biogeochemical Cycles*, *24*(1).
749   Emerson, S., & Hedges, J. (2008). *Chemical oceanography and the marine carbon cycle*.
750   Cambridge University Press.
751   Faassen, K. A. P., Nguyen, L. N. T., Broekema, E. R., Kers, B. A. M., Mammarella, I., Vesala,
752   T., Pickers, P. A., Manning, A. C., Vilà-Guerau de Arellano, J., Meijer, H. A. J., Peters,
753   W., & Luijkx, I. T. (2023). Diurnal variability of atmospheric O2, CO2, and their
754   exchange ratio above a boreal forest in southern Finland. *Atmos. Chem. Phys.*, *23*(2),
755   851-876. https://doi.org/10.5194/acp-23-851-2023
756   Falkowski, P. G. (1994). The role of phytoplankton photosynthesis in global biogeochemical
757   cycles. *Photosynthesis Research*, *39*(3), 235-258. https://doi.org/10.1007/BF00014586
758   Falkowski, P. G., & Raven, J. A. (2013). *Aquatic photosynthesis*. Princeton University Press.
759   Fay, A. R., Gregor, L., Landschützer, P., McKinley, G. A., Gruber, N., Gehlen, M., Iida, Y.,
760   Laruelle, G. G., Rödenbeck, C., Roobaert, A., & Zeng, J. (2021). SeaFlux: harmonization
761   of air–sea CO2 fluxes from surface pCO2 data products using a standardized approach.
762   *Earth Syst. Sci. Data*, *13*(10), 4693-4710. https://doi.org/10.5194/essd-13-4693-2021
763   Figuerola, B., Hancock, A. M., Bax, N., Cummings, V. J., Downey, R., Griffiths, H. J., Smith, J.,
764   & Stark, J. S. (2021). A Review and Meta-Analysis of Potential Impacts of Ocean
765   Acidification on Marine Calcifiers From the Southern Ocean [Review]. *Frontiers in*
766   *Marine Science*, *8*. https://doi.org/10.3389/fmars.2021.584445
767   Frankignoulle, M. (1994). A complete set of buffer factors for acid/base CO2 system in seawater.
768   *Journal of Marine Systems*, *5*(2), 111-118.
769   Fritsch, F. N., & Carlson, R. E. (1980). Monotone Piecewise Cubic Interpolation. *SIAM Journal*
770   *on Numerical Analysis*, *17*(2), 238-246. https://doi.org/10.1137/0717021
771   Fujii, M., Takao, S., Yamaka, T., Akamatsu, T., Fujita, Y., Wakita, M., Yamamoto, A., & Ono,
772   T. (2021). Continuous Monitoring and Future Projection of Ocean Warming,
773   Acidification, and Deoxygenation on the Subarctic Coast of Hokkaido, Japan [Original
774   Research]. *Frontiers in Marine Science*, *8*. https://doi.org/10.3389/fmars.2021.590020

775   Gattuso, J.-P., Magnan, A., Billé, R., Cheung, W. W., Howes, E. L., Joos, F., Allemand, D.,
776   Bopp, L., Cooley, S. R., & Eakin, C. M. (2015). Contrasting futures for ocean and society
777   from different anthropogenic CO2 emissions scenarios. *Science*, *349*(6243), aac4722.
778   Gruber, N., & Sarmiento, J. L. (2002). Large-scale biogeochemical-physical interactions in
779   elemental cycles. *The Sea*, *12*, 337-399.
780   Ho, D. T., Law, C. S., Smith, M. J., Schlosser, P., Harvey, M., & Hill, P. (2006). Measurements
781   of air-sea gas exchange at high wind speeds in the Southern Ocean: Implications for
782   global parameterizations. *Geophysical Research Letters*, *33*(16).
783   Hofmann, G. E., Smith, J. E., Johnson, K. S., Send, U., Levin, L. A., Micheli, F., Paytan, A.,
784   Price, N. N., Peterson, B., Takeshita, Y., Matson, P. G., Crook, E. D., Kroeker, K. J.,
785   Gambi, M. C., Rivest, E. B., Frieder, C. A., Yu, P. C., & Martz, T. R. (2011). High-
786   Frequency Dynamics of Ocean pH: A Multi-Ecosystem Comparison. *PLOS ONE*, *6*(12),
787   e28983. https://doi.org/10.1371/journal.pone.0028983
788   Humphreys, M. P., Lewis, E. R., Sharp, J. D., & Pierrot, D. (2022). PyCO2SYS v1.8: marine
789   carbonate system calculations in Python. *Geosci. Model Dev.*, *15*(1), 15-43.
790   https://doi.org/10.5194/gmd-15-15-2022
791   James, R. K., van Katwijk, M. M., van Tussenbroek, B. I., van der Heide, T., Dijkstra, H. A., van
792   Westen, R. M., Pietrzak, J. D., Candy, A. S., Klees, R., Riva, R. E. M., Slobbe, C. D.,
793   Katsman, C. A., Herman, P. M. J., & Bouma, T. J. (2020). Water motion and vegetation
794   control the pH dynamics in seagrass-dominated bays. *Limnology and Oceanography*,
795   *65*(2), 349-362. https://doi.org/https://doi.org/10.1002/lno.11303
796   Jiang, L.-Q., Carter, B. R., Feely, R. A., Lauvset, S. K., & Olsen, A. (2019). Surface ocean pH
797   and buffer capacity: past, present and future. *Scientific reports*, *9*(1), 1-11.
798   Jokiel, P. L., Jury, C. P., & Rodgers, K. S. (2014). Coral-algae metabolism and diurnal changes
799   in the CO2-carbonate system of bulk sea water. *PeerJ*, *2*, e378.
800   https://doi.org/10.7717/peerj.378
801   Jones, D. C., Ito, T., Takano, Y., & Hsu, W. C. (2014). Spatial and seasonal variability of the air-
802   sea equilibration timescale of carbon dioxide. *Global Biogeochemical Cycles*, *28*(11),
803   1163-1178.
804   Lee, K., Tong, L. T., Millero, F. J., Sabine, C. L., Dickson, A. G., Goyet, C., Park, G. H.,
805   Wanninkhof, R., Feely, R. A., & Key, R. M. (2006). Global relationships of total
806   alkalinity with salinity and temperature in surface waters of the world's oceans.
807   *Geophysical Research Letters*, *33*(19).
808   Li, A., Aubeneau, A. F., King, T., Cory, R. M., Neilson, B. T., Bolster, D., & Packman, A. I.
809   (2019). Effects of vertical hydrodynamic mixing on photomineralization of dissolved
810   organic carbon in arctic surface waters. *Environmental Science: Processes & Impacts*,
811   *21*(4), 748-760.
812   Martz, T. R., Connery, J. G., & Johnson, K. S. (2010). Testing the Honeywell Durafet® for
813   seawater pH applications. *Limnology and Oceanography: Methods*, *8*(5), 172-184.
814   https://doi.org/https://doi.org/10.4319/lom.2010.8.172
815   Middelburg, J. J., Soetaert, K., & Hagens, M. (2020). Ocean Alkalinity, Buffering and
816   Biogeochemical Processes. *Reviews of Geophysics*, *58*(3), e2019RG000681.
817   https://doi.org/10.1029/2019rg000681
818   Millero, F. J., & Poisson, A. (1981). International one-atmosphere equation of state of seawater.
819   *Deep Sea Research Part A. Oceanographic Research Papers*, *28*(6), 625-629.

820 Orr, J. C., Fabry, V. J., Aumont, O., Bopp, L., Doney, S. C., Feely, R. A., Gnanadesikan, A.,
821   Gruber, N., Ishida, A., Joos, F., Key, R. M., Lindsay, K., Maier-Reimer, E., Matear, R.,
822   Monfray, P., Mouchet, A., Najjar, R. G., Plattner, G.-K., Rodgers, K. B., . . . Yool, A.
823   (2005). Anthropogenic ocean acidification over the twenty-first century and its impact on
824   calcifying organisms. *Nature*, *437*(7059), 681-686. https://doi.org/10.1038/nature04095
825 Osborne, E. B., Thunell, R. C., Gruber, N., Feely, R. A., & Benitez-Nelson, C. R. (2020).
826   Decadal variability in twentieth-century ocean acidification in the California Current
827   Ecosystem. *Nature Geoscience*, *13*(1), 43-49. https://doi.org/10.1038/s41561-019-0499-z
828 Possenti, L., Humphreys, M. P., Bakker, D. C. E., Cobas-García, M., Fernand, L., Lee, G. A.,
829   Pallottino, F., Loucaides, S., Mowlem, M. C., & Kaiser, J. (2021). Air-Sea Gas Fluxes
830   and Remineralization From a Novel Combination of pH and O2 Sensors on a Glider
831   [Original Research]. *Frontiers in Marine Science*, *8*(1210).
832   https://doi.org/10.3389/fmars.2021.696772
833 Price, N. N., Martz, T. R., Brainard, R. E., & Smith, J. E. (2012). Diel Variability in Seawater pH
834   Relates to Calcification and Benthic Community Structure on Coral Reefs. *PLOS ONE*,
835   *7*(8), e43843. https://doi.org/10.1371/journal.pone.0043843
836 Qu, L., Xu, J., Sun, J., Li, X., & Gao, K. (2017). Diurnal pH fluctuations of seawater influence
837   the responses of an economic red macroalga Gracilaria lemaneiformis to future CO2-
838   induced seawater acidification. *Aquaculture*, *473*, 383-388.
839   https://doi.org/https://doi.org/10.1016/j.aquaculture.2017.03.001
840 Qu, T., & Lindstrom, E. J. (2004). Northward intrusion of Antarctic Intermediate Water in the
841   western Pacific. *Journal of Physical Oceanography*, *34*(9), 2104-2118.
842 Raven, J. A., & Johnston, A. M. (1991). Mechanisms of inorganic-carbon acquisition in marine
843   phytoplankton and their implications for the use of other resources. *Limnology and
844   Oceanography*, *36*(8), 1701-1714.
845 Richardson, D. J. (2000). Bacterial respiration: a flexible process for a changing environment.
846   *Microbiology*, *146*(3), 551-571.
847 Staudinger, C., Strobl, M., Breininger, J., Klimant, I., & Borisov, S. M. (2019). Fast and stable
848   optical pH sensor materials for oceanographic applications. *Sensors and Actuators B:
849   Chemical*, *282*, 204-217. https://doi.org/https://doi.org/10.1016/j.snb.2018.11.048
850 Staudinger, C., Strobl, M., Fischer, J. P., Thar, R., Mayr, T., Aigner, D., Müller, B. J., Müller, B.,
851   Lehner, P., Mistlberger, G., Fritzsche, E., Ehgartner, J., Zach, P. W., Clarke, J. S.,
852   Geißler, F., Mutzberg, A., Müller, J. D., Achterberg, E. P., Borisov, S. M., & Klimant, I.
853   (2018). A versatile optode system for oxygen, carbon dioxide, and pH measurements in
854   seawater with integrated battery and logger. *Limnology and Oceanography: Methods*,
855   *16*(7), 459-473. https://doi.org/https://doi.org/10.1002/lom3.10260
856 Stoll, M., Bakker, K., Nobbe, G., & Haese, R. (2001). Continuous-flow analysis of dissolved
857   inorganic carbon content in seawater. *Analytical Chemistry*, *73*(17), 4111-4116.
858 Strickland, J. D. H., & Parsons, T. R. (1972). A practical handbook of seawater analysis.
859 Stumm, W., & Morgan, J. J. (2012). *Aquatic chemistry: chemical equilibria and rates in natural
860   waters*. John Wiley & Sons.
861 Sulpis, O., Lauvset, S. K., & Hagens, M. (2020). Current estimates of K1* and K2* appear
862   inconsistent with measured CO2 system parameters in cold oceanic regions. *Ocean Sci.*,
863   *16*(4), 847-862. https://doi.org/10.5194/os-16-847-2020
864 Sutton, A. J., Feely, R. A., Maenner-Jones, S., Musielwicz, S., Osborne, J., Dietrich, C.,
865   Monacci, N., Cross, J., Bott, R., Kozyr, A., Andersson, A. J., Bates, N. R., Cai, W. J.,

866   Cronin, M. F., De Carlo, E. H., Hales, B., Howden, S. D., Lee, C. M., Manzello, D. P., . .
867   . Weller, R. A. (2019). Autonomous seawater pCO2 and pH time series from 40 surface
868   buoys and the emergence of anthropogenic trends. *Earth Syst. Sci. Data*, *11*(1), 421-439.
869   https://doi.org/10.5194/essd-11-421-2019
870 Uppström, L. R. (1974). The boron/chlorinity ratio of deep-sea water from the Pacific Ocean.
871   *Deep Sea Research and Oceanographic Abstracts*, *21*(2), 161-162.
872   https://doi.org/https://doi.org/10.1016/0011-7471(74)90074-6
873 Vallis, G. K. (2017). *Atmospheric and oceanic fluid dynamics*. Cambridge University Press.
874 Wang, X., Yin, Z., Chen, J., & Liu, J. (2023). Phytoplankton Carbon Utilization Strategies and
875   Effects on Carbon Fixation. *Water*, *15*(11), 2137. https://www.mdpi.com/2073-
876   4441/15/11/2137
877 Wei, Z., Zhang, Y., Yang, F., & Long, L. (2022). Diurnal fluctuations in seawater pCO2 amplify
878   the negative effects of ocean acidification on the biotic performance of the calcifying
879   macroalga Halimeda opuntia [Original Research]. *Frontiers in Marine Science*, *9*.
880   https://doi.org/10.3389/fmars.2022.968740
881 Wu, Y., Hain, M. P., Humphreys, M. P., Hartman, S., & Tyrrell, T. (2019). What drives the
882   latitudinal gradient in open-ocean surface dissolved inorganic carbon concentration?
883   *Biogeosciences*, *16*(13), 2661-2681. https://doi.org/10.5194/bg-16-2661-2019
884 Zeebe, R. E., & Wolf-Gladrow, D. A. (2001). *CO2 in seawater: equilibrium, kinetics, isotopes*.
885   http://site.ebrary.com/id/10190754
886 Zehr, J. P., & Kudela, R. M. (2011). Nitrogen cycle of the open ocean: from genes to
887   ecosystems. *Annual Review of Marine Science*, *3*, 197-225.
888
889